with the observation. The fitness of each individual is quantified by χ^2. Children are then created by choosing one parent individual and calculating the second one from three randomly chosen individuals according to

$$p'_c = p_c + f_{\rm m}(p_a - p_b), \qquad (4.2.7.5)$$

where $f_{\rm m}$ governs the mutations. The chromosome of the child is obtained by combining the genes of the two parents governed by a crossover (or recombination) constant $f_{\rm r}$. If its fitness is higher than that of the parent, it replaces it. This procedure is repeated until some convergence criterion is reached. This DE method is still rather time-consuming on the computer. Therefore, the CE technique was introduced, where only one crystal is built up during the refinement. Here a large population is created spanning a large but reasonable parameter space. Individuals are selected at random to decide upon acceptance or rejection of an MC move *via* their own energy criteria. Then χ^2 is calculated and according to its positive or negative change a gratification or penalty weight is given to that individual. It may live as long as this weight is positive, otherwise it is replaced by a new individual calculated from (4.2.7.5). This way, useful individuals live longer to act on the same crystal, while unsuccessful ones are eliminated early. Note that the recombination operation is not used in this technique.

(4) *The PDF method*. The pair-distribution function (PDF) has long been used for the analysis of liquids, glasses and amorphous substances (Warren, 1969), but has recently regained considerable interest for the analysis of crystalline substances as well (Egami, 1990; Billinge & Egami, 1993; Egami, 2004). The PDF is obtained by a Fourier transformation of the total (Bragg plus diffuse) scattering in a powder pattern,

$$\rho_0 G(r) = \rho_0 + \tfrac{1}{2}\int H[S(H) - 1]\sin(2\pi H)\ {\rm d}H. \qquad (4.2.7.6)$$

This is nothing other than the van Hove correlation function (4.2.2.2) or the related Patterson function (4.2.2.5) averaged spherically and taken at $t = 0$ (a snapshot) and is given by

$$G^{\rm PDF}(r) = 4\pi r[\rho(r) - \rho_0] = \left(\sum c_i b_i\right)^{-2} 4\pi r \rho_0 G(r), \qquad (4.2.7.7)$$

where ρ_0 is the average number density and

$$\rho(r) = (1/N)\sum (b_i b_{i'}/\langle b\rangle^2)\delta(r - r_{ii'}). \qquad (4.2.7.8)$$

The δ functions are then convoluted with a normalized Gaussian to account for (harmonic) thermal motion. Parameter refinement proceeds in a similar way to the RMC technique. First a model is built, initially within just one unit cell and with periodic boundary conditions, then its PDF is calculated, compared with the observed one and further improved using, for example, MC simulated annealing. The model is then enlarged to include longer-range correlations. Owing to the small size of the models, this technique is much faster than the RMC method. It is essential, however, that data are measured up to very high H values to minimize truncation errors in (4.2.7.6).

4.2.7.3.3. General remarks

All of the different modelling techniques mentioned in this section have their specific merits and limitations and have contributed much to our understanding of disorder in crystalline materials following the interpretation of the corresponding diffuse scattering. It should be borne in mind, however, that application of these methods is still far from being routine work and it requires a lot of intuition to ensure that the final model is physically and chemically reasonable. In particular, it must always be ensured that the average structure remains consistent with that derived from the Bragg reflections alone. This may be done by keeping the Bragg reflections, *i.e.* by analysing the total scattering, or by designing special algorithms, *e.g.* by swapping two atoms at the same time (Proffen & Welberry, 1997). Moreover, possible traps and corrections like local minima, termination errors, instrumental resolution, statistical noise, inelasticity *etc*. must be carefully considered. All this means that the analytical methods outlined in Section 4.2.5 keep their value and should be preferred wherever possible.

The newly emerging technique of using full quantum-mechanical *ab initio* calculations for structure predictions along with MD simulations may also be applied to disordered systems. The limited currently available computer power, however, restricts this possibility to rather simple systems and small simulation box sizes, but, with the expected further increase of computer capacities, this may open up new perspectives for the future.

4.2.8. Experimental techniques and data evaluation

Single-crystal and powder diffractometry are used in diffuse scattering work. Conventional and more sophisticated special techniques and instruments are now available at synchrotron facilities and modern neutron reactor and spallation sources. The full merit of the dedicated machines may be assessed by inspecting the corresponding handbooks, which are available upon request from the facilities. In the following, some common important aspects that should be considered when planning and performing a diffuse-scattering experiment are summarized and a short overview of the techniques is given. Methodological aspects of diffuse scattering at low angles, *i.e.* small-angle-scattering techniques, and high-resolution single-crystal diffractometers are excluded. Instruments of the latter type are used when diffuse intensities beneath Bragg reflections or reflection profiles and tails must be analysed to study long-range distortion fields around single defects or small defect aggregates. In the case of small defect concentrations, the crystal structure remains almost perfect and the dynamical theory of diffraction is more appropriate. This topic is beyond the scope of this chapter.

4.2.8.1. Single-crystal techniques

In general, diffuse scattering is weak in comparison with Bragg scattering, and is anisotropically and inhomogeneously distributed in reciprocal space. The origin may be a static phenomenon or a dynamic process, giving rise to elastic or inelastic (quasi-elastic) diffuse scattering, respectively. If the disorder problem relates to more than one structural element, different parts of the diffuse scattering may show different behaviour in reciprocal space and/or on an energy scale. Therefore, before starting an experiment, some principal aspects should be considered: Is there need for X-ray and/or neutron methods? What is the optimum wavelength or energy (band), or does a 'white' technique offer advantages? Can focusing techniques be used without too strong a loss of resolution and what are the best scanning procedures? How can the background be minimized? Has the detector a low intrinsic noise and a high dynamic range?

On undertaking an investigation of a disorder problem by an analysis of the diffuse scattering, an overall picture should first be recorded by X-ray diffraction. Several sections through reciprocal space help to define the problem. For this purpose 'old-fashioned' film methods may be used, where the classical film is now commonly replaced by an imaging plate (IP) or a charge-coupled device (CCD) camera (see below). Clearly, short crystal-to-detector distances provide larger sections and avoid long exposure times, but suffer from spatial resolution. Distorted sections through the reciprocal lattice, such as produced by the Weissenberg method, may be transformed into a form suitable for easy interpretation (Welberry, 1983). The transformation of diffuse data measured using an IP or CCD requires suitable

software for the specific type of detector and is not always routinely available (Estermann & Steurer, 1998).

Standing-crystal techniques in combination with monochromatic radiation, usually called monochromatic Laue techniques (see, *e.g.*, Flack, 1970), save exposure time, which is particularly interesting for 'in-house' laboratory diffuse X-ray work. The Noromosic technique (Jagodzinski & Korekawa, 1973) is characterized by a convergent monochromatic beam which simulates an oscillation photograph over a small angular range. Heavily overexposed images, with respect to Bragg scattering, allow for sampling of diffuse intensity if a crystal is oriented in such a way that there is a well defined section between the Ewald sphere and the diffuse phenomenon under consideration. By combining single Noromosic photographs, Weissenberg patterns can be simulated. This relatively tedious method is often unavoidable because the heavily overexposed Bragg peaks obscure weak diffuse phenomena. Furthermore, standing pictures at distinct crystal settings in comparison with conventional continuous recording are frequently sufficient in diffuse scattering work and save time. Long-exposure Weissenberg photographs are therefore not equivalent to a smaller set of standing photographs. In this context it should be mentioned that a layer-line screen has not only the simple function of a selecting diaphragm, but the gap width determines the resolution volume within which diffuse intensity is collected (Welberry, 1983). For further discussion of questions of resolution see below. A comparison of Weissenberg and diffractometer methods for the measurement of diffuse scattering is given by Welberry & Glazer (1985). It should be pointed out, however, that diffractometer methods at synchrotron sources become more widely used if only very small (micrometre-sized) single-crystal specimens have to be used to study a disorder problem.

The basic arguments for using neutron-diffraction methods were given in Section 4.2.2.2: (i) the different interactions of X-rays and neutrons with matter; (ii) the lower absorption of neutrons, in particular when using longer (> 0.15 nm) wavelengths; and (iii) the matching of the energy of thermal neutrons with that of the phonons that contribute to the TDS background, and, in consequence, to separate it by a 'purely' elastic measurement. A comparative consideration of synchrotron- and neutron-related diffuse work on disordered alloys is given by Schweika (1998). Specific aspects of neutron diffraction and instruments are discussed at the end of this section.

Intensities: As mentioned above, diffuse intensities are usually weaker by several orders of magnitude than Bragg data. Therefore intense radiation sources are needed. Even a modern X-ray tube is a stronger source, defined by the flux density from the anode (number of photons $\mathrm{cm}^{-2}\,\mathrm{s}^{-1}$), than modern neutron sources. For this reason most experimental work which can be performed with X-rays should be. In home laboratories the intense characteristic spectrum of an X-ray tube is commonly used. At synchrotron storage rings any wavelength from a certain range can be selected. The extremely high brilliance (number of quanta cm^{-2}, sr^{-1}, s^{-1} and wavelength interval) of modern synchrotron sources is, however, unnecessary in the case of slowly varying diffuse phenomena. In these cases, an experimental setup at a laboratory rotating anode is competitive and often even superior if specimens with sufficient size are available. Various aspects of diffuse X-ray work at a synchrotron facility are discussed by Matsubara & Georgopoulos (1985), Oshima & Harada (1986) and Ohshima *et al.* (1986). Diffuse neutron-diffraction work can only be performed on a high-flux reactor or on a powerful spallation source. Highly efficient monochromator systems are needed when using a crystal diffractometer. Time-of-flight (TOF) neutron diffractometers at pulsed (spallation) neutron sources are equivalent to conventional diffractometers at reactors (Windsor, 1982). The merits of diffuse neutron work at pulsed sources have been discussed by Nield & Keen (2001).

Wavelength: The choice of an optimum wavelength is important with respect to the problem to be solved. For example, point defects cause diffuse scattering to fall off with increasing scattering vector; short-range ordering between clusters causes broad peaks corresponding to large d spacings; lattice-relaxation processes induce a broadening of the interferences; static modulation waves with long periods give rise to satellite scattering close to Bragg peaks. In all these cases, a long wavelength is preferable due to the higher resolution. The use of a long wavelength is also profitable when the main diffuse contributions can be recorded within an Ewald sphere as small as the Bragg cutoff of the sample at $H \simeq 1/(2d_{\max})$. 'Contamination' by Bragg scattering can thus be avoided. This is also advantageous from a different point of view: because the contribution of thermal diffuse scattering increases with increasing scattering vector $\mathbf{H}$, the relative amount of this component becomes negligibly small within the first reciprocal cell. However, one has to take care with the absorption of long-wavelength neutrons.

On the other hand, short wavelengths are needed where atomic displacements play the dominant role. If diffuse peaks in large portions of the reciprocal space, or diffuse streaks or planes, have to be recorded up to high values of the scattering vector in order to decide between different structural disorder models, hard X-rays or hot neutrons are needed. For example, high-energy X-rays (65 keV) provided at a synchrotron source were used by Welberry *et al.* (2003) to study diffuse diffraction from ceramic materials and allowed studies with better d resolution.

The λ^3 dependence of the scattered intensity, in the framework of the kinematical theory, is a crucial point for exposure or data-acquisition times. Moreover, the accuracy with which an experiment can be carried out suffers from a short wavelength: generally, momentum as well as energy resolution are lower. For a quantitative estimate detailed considerations of resolution in reciprocal space (and energy) are needed.

A specific wavelength aspect concerns the method of (X-ray) anomalous dispersion, which may also be used in diffuse-scattering work. It allows the contrast and identification of certain elements in a disordered structure. Even small concentrations of impurity atoms or defects as low as 10^{-6} can be determined by this method if the impurity atoms are located at specific sites, *e.g.* in domain boundaries, or if certain other defect structures exist with characteristic diffuse scattering in reciprocal space. The (weak) diffuse scattering can then be contrasted by tuning the wavelength across an absorption edge of the particular atomic species. To avoid strong fluorescence background scattering such an experiment is usually performed at different wavelengths (energies) at the 'low absorption side' close to an edge. The merit of this method was demonstrated by Berthold & Jagodzinski (1990), who analysed diffuse streaks due to boundaries between lamellar domains in an albite feldspar. Similar element contrast can be achieved in neutron diffuse work if using specimens with different isotopes, *e.g.* H–D exchange.

Monochromacy: In classical crystal diffractometry, monochromatic radiation is used in order to eliminate broadening effects due to the wavelength distribution. Focusing monochromators and other focusing devices (guides, mirrors) help to overcome the lack of luminosity. A focusing technique is very helpful for deciding between geometrical broadening and 'true' diffuseness. In a method that is used with some success, the sample is placed in a monochromatic divergent beam with its selected axis lying in the scattering plane of the monochromator (Jagodzinski, 1968). The specimen is fully embedded in the incident beam, which is focused onto a 2D detector. Using this procedure the influence of the sample size is suppressed in one dimension. In white-beam (neutron) time-of-flight diffractometry the time resolution is the counterpart to the wavelength resolution. This is discussed in some detail in the textbook of Keen & Nield (2004).

Detectors: Valuable developments with a view to diffuse-scattering work are multidetectors (see, *e.g.*, Haubold, 1975) and position-sensitive detectors for X-rays (Arndt, 1986*a*,*b*) and neutrons (Convert & Forsyth, 1983). A classical '2D area detector' is the photographic film – nowadays of less importance – which has to be 'read out' by microdensitometer scanning. Important progress in recording diffuse X-ray data has been made by the availability of multiwire detectors, IPs and CCD cameras (Estermann & Steurer, 1998). For 2D position-sensitive (proportional) counters problems may arise from inhomogeneities of the wire array as well as the limited dynamic range when a Bragg reflection is accidentally recorded. IP systems have the major advantage of a larger dynamic range, 10^5–10^6, compared to 10^2–10^3 for an X-ray film. IPs can also be used in diffuse experiments carried out with hard (65 keV) X-rays (Welberry *et al.*, 2003). IPs are also available for neutron work, where the necessary transformation of the detected neutrons into light signals is provided by special neutron-absorbing converter foils (Niimura *et al.*, 2003). The problem of an intrinsic sensitivity to gamma radiation may be overcome by protection with a thin sheet of lead. IPs allow data collection either in plane geometry or in simple rotation or Weissenberg geometry, both in combination with low- and high-temperature devices. CCD detectors are well suited for X-ray diffuse scattering, and when used in combination with converter foils they can also be used for the detection of neutrons. A basic prerequisite is a low intrinsic noise, which can be achieved by cooling the CCD with liquid nitrogen. With these detectors, extended diffuse data sets can be collected by rotating the sample in distinct narrow steps around a spindle axis over several χ settings and subsequent oscillations over a small angular range. Thus large parts of the reciprocal space can be recorded. An example is given by Campbell *et al.* (2004), who studied subtle defect structures in the microporous framework material mordenite. Linear position-sensitive detectors are mainly used in powder work, but can also be used for recording diffuse scattering by single crystals. By combining a linear position-sensitive detector and the TOF method, a whole area in reciprocal space is accessible simultaneously (Niimura *et al.*, 1982; Niimura, 1986).

Diffuse data recorded with IPs or CCDs are commonly evaluated by commercial software supplied by the manufacturer. These software packages include corrections for extracted Bragg data, but no special software tools for treating extended (diffuse) data are commonly available. One particular problem relates to the background definition for diffuse IP data. Even after subtraction of electronic noise, there remains considerable uncertainty about the amount of true background scattering from the sample as recorded by an IP scanner. The definitions of errors and error maps remain doubtful as long as the true conversion rate between the captured neutron or photon *versus* the recorded optical signal is unknown.

Absorption: Special attention must be paid to absorption phenomena, in particular when (in the X-ray case) an absorption edge of an element of the sample is close to the wavelength. Then strong fluorescence scattering may completely obscure weak diffuse-scattering phenomena. In comparison with X-rays, the generally lower absorption coefficients of neutrons make absolute measurements easier. This also allows the use of larger sample volumes, which is not true in the X-ray case. Moreover, the question of sample environment is less serious in the neutron case than in the X-ray case. However, the availability of hard X-rays at a synchrotron source (Butler *et al.*, 2000; Welberry *et al.*, 2003) makes the X-ray absorption problem less serious: irregularly shaped specimens without special surface treatment could be used. There is also no need for complicated absorption corrections and the separation of fluorescence background is rather simple.

Extinction: An extinction problem does not generally exist in diffuse-scattering work.

Background: An essential prerequisite for a diffuse-scattering experiment is the careful suppression of background scattering. Incoherent X-ray scattering by a sample gives continuous blackening in the case of fluorescence, or scattering at high 2θ angles owing to Compton scattering or 'incoherent' inelastic effects. Protecting the image plate with a thin Al or Ni foil is of some help against fluorescence, but also attenuates the diffuse intensity. Obviously, energy-dispersive counter methods are highly efficient in this case (see below). Air scattering produces a background at low 2θ angles which may easily be avoided by special slit systems and evacuation of the camera.

In X-ray or neutron diffractometer measurements, incoherent and multiple scattering contribute to a background which varies only slowly with 2θ and can be subtracted by linear interpolation or fitting a smooth curve, or can even be calculated quantitatively and then subtracted. In neutron diffraction there are rare cases when monoisotopic and 'zero-nuclear-spin' samples are available and, consequently, the corresponding incoherent scattering part vanishes completely. In some cases, a separation of coherent and incoherent neutron scattering is possible by polarization analysis (Gerlach *et al.*, 1982). An 'empty' scan can take care of instrumental background contributions. Evacuation or controlled-atmosphere studies need a chamber, which may give rise to spurious scattering. This can be avoided if no part of the vacuum chamber is hit by the primary beam. The problem is less serious in neutron work. The mounting of the specimen, *e.g.*, on a silica fibre with cement, poorly aligned collimators and beam catchers are further sources. Sometimes a specimen has to be enclosed in a capillary, which will always be hit by the incident beam. Careful and tedious experimental work is necessary in the case of low- and high-temperature (or -pressure) investigations, which have to be carried out in many disorder problems. While the experimental situation is again less serious in neutron scattering, there are problems with scattering from walls and containers in X-ray work. Because TDS dominates at high temperatures and in the presence of a static disorder problem, a quantitative separation can rarely be carried out in the case of high experimental background. Calculation and subtraction of the TDS is possible in principle, but difficult in practice. If the disorder problem in which one is interested in does not change with temperature, a low-temperature experiment can be carried out. Another way to get rid off TDS, at least partly, is by using a neutron diffractometer with an additional analyser set to zero-energy transfer.

Resolution: A quantitative analysis of diffuse-scattering data is essential for reaching a definite decision about a disorder model, but – in many cases – it is cumbersome. By comparing the calculated and corrected experimental data the magnitudes of the parameters of the structural disorder model may be derived. A careful analysis of the data requires, therefore, after separation of the background (see above), corrections for polarization (in the X-ray case), absorption (in conventional X-ray work) and resolution. Detailed considerations of instrumental resolution are necessary; the resolution depends, in addition to other factors, on the scattering angle and implies intensity corrections analogous to the Lorentz factor used in structure analysis from sharp Bragg reflections.

Resolution is conveniently described by the function $R(\mathbf{H}-\mathbf{H}_0)$, which is defined as the probability of detecting a photon or neutron with momentum transfer $h\mathbf{H} = h(\mathbf{k}-\mathbf{k}_0)$ when the instrument is set to measure $\mathbf{H}_0$. This function R depends on the instrumental parameters (such as the collimations, the mosaic spread of monochromator and the scattering angle) and the spectral width of the source. Fig. 4.2.8.1 shows a schematic sketch of a diffractometer setting. Detailed considerations of resolution volume in X-ray and neutron diffractometry are given by Sparks & Borie (1966) and by Cooper & Nathans (1968*a*,*b*), respectively. If a triple-axis (neutron) instrument is used, for example in a purely elastic configuration, the set of instrumental parameters includes the mosaicity of the analyser

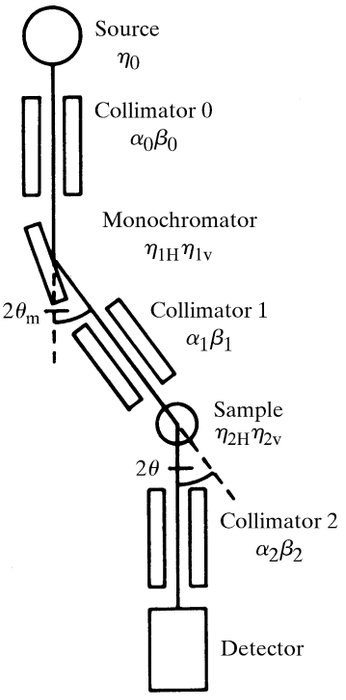

Fig. 4.2.8.1. Schematic sketch of a diffractometer setting.

and the collimations between the analyser and detector. In general, Gaussians are assumed to parameterize the mosaic distributions and transmission functions. Sophisticated resolution-correction programs are usually provided at any standard instrument for carrying out experiments at synchrotron and neutron facilities.

The general assumption of Gaussians is not too serious in the X-ray case (Iizumi, 1973). Restrictions are due to absorption, which makes the profiles asymmetric. Box-like functions are considered to be better for the spectral distribution or for large apertures (Boysen & Adlhart, 1987). These questions are treated in some detail by Klug & Alexander (1954). The main features, however, may also be derived by the Gaussian approximation. In practice, the function R may be obtained either by calculation from the known instrumental parameters or by measuring Bragg peaks from a perfect unstrained crystal. In the latter case, the intensity profile is given solely by the resolution function. Normalization with the Bragg intensities is also useful in order to place the diffuse-scattering intensity on an absolute scale.

In conventional single-crystal diffractometry the measured intensity is given by the convolution product of $\mathrm{d}\sigma/\mathrm{d}\Omega$ with R,

$$I(\mathbf{H}_0) = \int \frac{\mathrm{d}\sigma}{\mathrm{d}\Omega}(\mathbf{H})[R(\mathbf{H}-\mathbf{H}_0)]\,\mathrm{d}\mathbf{H}, \tag{4.2.8.1}$$

where $\mathrm{d}\sigma/\mathrm{d}\Omega$ describes the scattering cross section for the disorder problem. In a more accurate form the mosaicity of the sample has to be included:

$$\begin{aligned} I(\mathbf{H}_0) &= \int \frac{\mathrm{d}\sigma}{\mathrm{d}\Omega}(\mathbf{H}-\Delta\mathbf{K})[\eta(\Delta\mathbf{K})R(\mathbf{H}-\mathbf{H}_0)]\,\mathrm{d}\mathbf{H}\,\mathrm{d}(\Delta\mathbf{K}) \\ &= \int \frac{\mathrm{d}\sigma}{\mathrm{d}\Omega}(\mathbf{H}')[R'(\mathbf{H}'-\mathbf{H}_0)]\,\mathrm{d}\mathbf{H}'. \end{aligned} \tag{4.2.8.1a}$$

$R'(\mathbf{H}'-\mathbf{H}_0) = \int \eta(\Delta\mathbf{K})R(\mathbf{H}'+\Delta\mathbf{K}-\mathbf{H}_0)\,\mathrm{d}(\Delta\mathbf{K})$. The mosaic block distribution around a most probable vector $\mathbf{K}_0$ is described by $\eta(\Delta\mathbf{K})$: $\Delta\mathbf{K} = \mathbf{K}-\mathbf{K}_0$; $\mathbf{H}' = \mathbf{H}-\Delta\mathbf{K}$.

In (4.2.8.1) all factors independent of 2θ are neglected. All intensity expressions have to be calculated from equations (4.2.8.1) or (4.2.8.1a).

The intensity variation of diffuse peaks with 2θ measured with a single detector was studied in detail by Yessik *et al.* (1973). In principle, all special cases are included there. In practice, however, some important simplifications can be made if $\mathrm{d}\sigma/\mathrm{d}\Omega$ is either very broad or very sharp compared with R, *i.e.* for Bragg peaks, sharp streaks, 'thin' diffuse layers or extended 3D diffuse peaks (Boysen & Adlhart, 1987).

In the latter case, the cross section $\mathrm{d}\sigma/\mathrm{d}\Omega$ may be treated as nearly constant over the resolution volume so that the corresponding 'Lorentz' factor is independent of 2θ:

$$L_{3\mathrm{D}} = 1. \tag{4.2.8.2}$$

For a diffuse plane within the scattering plane with very small thickness and slowly varying cross section within the plane, one derives for a point measurement in the plane

$$L_{2\mathrm{D},\parallel} = (\beta_1'^2 + \beta_2^2 + 4\eta_{2\mathrm{v}}^2\sin^2\theta)^{-1/2}, \tag{4.2.8.3}$$

exhibiting an explicit dependence on θ (β_1', β_2 and $\eta_{2\mathrm{v}}$ determine an effective vertical divergence before the sample, the divergence before the detector and the vertical mosaic spread of the sample, respectively).

In the case of *relaxed* vertical collimations $\beta_1', \beta_2 \gg \eta_{2\mathrm{v}}$

$$L_{2\mathrm{D},\parallel} = (\beta_1'^2 + \beta_2^2)^{-1/2}, \tag{4.2.8.3a}$$

i.e. again independent of θ.

Scanning across the diffuse layer in a direction perpendicular to it one obtains an integrated intensity which is also independent of 2θ. This is even true if approximations other than Gaussians are used.

If, on the other hand, an equivalent diffuse plane is positioned perpendicular to the scattering plane, the equivalent expression for $L_{2\mathrm{D},\perp}$ of a point measurement is given by

$$\begin{aligned} L_{2\mathrm{D},\perp} \simeq [&4\eta_{2\mathrm{H}}^2\sin^2\theta\cos^2\psi + \alpha_2^2\sin^2(\psi-\theta) \\ &+ \alpha_1'^2\sin^2(\psi+\theta) + 4\eta_0'\sin^2\theta\sin^2\psi \\ &- 4\alpha_1''\sin\theta\sin\psi\sin(\theta+\psi)], \end{aligned} \tag{4.2.8.4}$$

where ψ gives the angle between the vector $\mathbf{H}_0$ and the line of intersection between the diffuse plane and the scattering plane. The coefficients $\eta_{2\mathrm{H}}$, α_2, α_1', α_1'' and η are either instrumental parameters or functions of them, defining horizontal collimations and mosaic spreads. In the case of a sharp X-ray line (produced, for example, by filtering) the last two terms in equation (4.2.8.4) vanish.

The use of integrated intensities from individual scans perpendicular to the diffuse plane, now carried out within the scattering plane, again gives a Lorentz factor independent of 2θ.

In the third fundamental special case, diffuse streaking along one reciprocal direction within the scattering plane (with a narrow cross section and slowly varying intensity along the streak), the Lorentz factor for a point measurement may be expressed by the product

$$L_{1\mathrm{D},\parallel} \simeq L_{2\mathrm{D},\parallel}L_{2\mathrm{D},\perp}, \tag{4.2.8.5}$$

where ψ now defines the angle between the streak and $\mathbf{H}_0$. The integrated intensity taken from an H scan perpendicular to the streak has to be corrected by a Lorentz factor which is equal to $L_{2\mathrm{D},\parallel}$ [equation (4.2.8.3)]. In the case of a diffuse streak perpendicular to the scattering plane, a relatively complicated equation holds for the corresponding Lorentz factor (Boysen & Adlhart, 1987). Again, simpler expressions hold for integrated intensities from H scans perpendicular to the streaks. Such scans may be performed in the radial direction (corresponding to a θ–2θ scan),

$$L_{1\mathrm{D},\perp,\mathrm{rad}} = (4\eta_{2\mathrm{H}}^2 + \alpha_2^2 + \alpha_1'^2)^{-1/2}(1/\sin\theta), \tag{4.2.8.6}$$

or perpendicular to the radial direction (within the scattering plane) (corresponding to an ω scan),

$$L_{1\mathrm{D},\perp,\mathrm{per}} = (\alpha_2^2 + \alpha_1^2 + 4\eta_0' \tan^2\theta - 4\alpha_1'' \tan\theta)^{-1/2}(1/\cos\theta). \quad (4.2.8.7)$$

Note that only the radial scan yields a simple θ dependence ($\sim 1/\sin\theta$).

From these considerations it is recommended that integrated intensities from scans perpendicular to a diffuse plane or a diffuse streak should be used in order to extract the disorder cross sections. For other scan directions, which make an angle α with the intersection line (diffuse plane) or with a streak, the L factors are simply $L_{2\mathrm{D},\perp}/\sin\alpha$ and $L_{1\mathrm{D},\perp}/\sin\alpha$, respectively.

One point should be emphasized: since in a usual experiment with a single counter the integration is performed over an angle $\Delta\omega$ *via* a general $\delta\omega{:}(g\delta 2\theta)$ scan, an additional correction factor arises:

$$\Delta\omega/\Delta\mathbf{H}_\beta = \sin(\beta+\theta)/(\mathbf{k}_0 \sin 2\theta). \quad (4.2.8.8)$$

β is the angle between $\mathbf{H}_0$ and the scan direction $\mathbf{H}_\beta$, and $g = (\tan\beta + \tan\theta)/(2\tan\theta)$ defines the coupling ratio between the rotation of the crystal around a vertical axis and the rotation of the detector shaft. The so-called 1:2 and ω-scan techniques are most frequently used, where $\beta = 0$ and 90°, respectively.

White-beam techniques: Techniques for the measurement of diffuse scattering using a *white* spectrum are common in neutron diffraction. Owing to the relatively low velocity of thermal or cold neutrons, TOF methods in combination with time-resolving detector systems placed at a fixed angle 2θ allow for a simultaneous recording along a radial direction through the origin of reciprocal space (see, *e.g.*, Turberfield, 1970; Bauer *et al.*, 1975). The scan range is limited by the Ewald spheres corresponding to $\lambda_{\max}$ and $\lambda_{\min}$, respectively. With several such detector systems placed at different angles or a 2D detector several scans may be carried out simultaneously during one neutron pulse.

An analogue of neutron TOF diffractometry in the X-ray case is a combination of a white source of X-rays and an energy-dispersive detector. This technique, which has been known in principle for a long time, suffered from relatively weak white sources. With the development of high-power X-ray generators and synchrotron sources this method has now become highly interesting. Its use in diffuse-scattering work (in particular, the effects on resolution) is discussed by Harada *et al.* (1984).

Some examples of neutron instruments dedicated to diffuse scattering are the diffractometers D7 at the Institut Laue–Langevin (ILL, Grenoble), DNS at the Forschungsneutronenquelle Heinz Maier-Leibnitz (FRM-II, Munich), G4-4 at the Laboratoire Léon Brillouin (LLB, Saclay) or SXD at ISIS, Rutherford Appleton Laboratory (RAL, UK). The instrument DNS uses a polarization analysis for diffuse scattering (Schweika & Böni, 2001; Schweika, 2003) and the SXD diffractometer is a TOF instrument using a (pulsed) white beam (Keen & Nield, 2004). All these instruments are equipped with banks of detectors. The single-crystal diffractometer D19 at the ILL, equipped with a multiwire area detector, is also suitable for collecting diffuse data. The flat-cone machine E2 at the Hahn–Meitner Institut (HMI, Berlin) is equipped with a bank of area detectors, has an option to record higher-order layers and can also be operated in an 'elastic' mode with a multicrystal analyser. The instrument D10 at the ILL is a versatile instrument which can be operated as a low-background two-axis or three-axis diffractometer with several further options. Neutron diffractometers that have recently become operational are BIX-3 at the Japan Atomic Energy Research Institute (JAERI, Japan), LADI at the ILL, where neutron-sensitive IPs are used for macromolecular work (for a comparison see Niimura *et al.*, 2003), and RESI at the Forschungsneutronenquelle Heinz Maier-Leibnitz (FRM-II, Munich) for common solid-state investigations. Information about all these instruments can be found in the respective handbooks or on the websites of the facilities.

4.2.8.2. Powders and polycrystals

The diffuse background in powder diagrams also contains valuable information about disorder. Only in very simple cases can a model be deduced from a powder pattern alone, but a refinement of a known disorder model can favourably be carried out, *e.g.* the temperature dependence may be studied. On account of the intensity integration, the ratio of diffuse intensity to Bragg intensity is enhanced in a powder pattern. Moreover, a powder pattern contains, in principle, all the information about the sample and might thus reveal more than single-crystal work. However, in powder-diffractometer experiments preferred orientations and textures could lead to a complete misidentification of the problem. Single-crystal experiments are generally preferable in this respect. Nevertheless, high-resolution powder investigations may give quick supporting information, *e.g.* about superlattice peaks, split reflections, lattice strains, domain-size effects, lattice-constant changes related to a disorder effect *etc*.

Evaluation of diffuse-scattering data from powder diffraction follows the same theoretical formulae developed for the determination of the radial distribution function for glasses and liquids. The final formula for random distributions may be given as (Fender, 1973)

$$I_D^p = \{\langle|F(\mathbf{H})|^2\rangle - |\langle F(\mathbf{H})\rangle|^2\} \sum_i s_i \sin(2\pi H r_i)/(2\pi H r_i). \quad (4.2.8.9)$$

s_i represents the number of atoms at distance r_i from the origin. An equivalent expression for a substitutional binary alloy is

$$I_D^p = \alpha(1-\alpha)\{|f_2(\mathbf{H}) - f_2(\mathbf{H})|^2\} \sum_i s_i \sin(2\pi H r_i)/(2\pi H r_i). \quad (4.2.8.10)$$

A quantitative calculation of a diffuse background is also helpful in combination with Rietveld's method (1969) for refining an averaged structure by fitting Bragg data. In particular, for highly anisotropic diffuse phenomena characteristic asymmetric line shapes occur.

The calculation of these line shapes is treated in the literature, mostly neglecting the instrumental resolution (see, *e.g.*, Warren, 1941; Wilson, 1949; Jones, 1949; and de Courville-Brenasin *et al.*, 1981). This is not justified if the variation of the diffuse intensity becomes comparable with that of the resolution function, as is often the case in neutron diffraction. The instrumental resolution may be incorporated using the resolution function of a powder instrument (Caglioti *et al.*, 1958). A detailed analysis of diffuse peaks is given by Yessik *et al.* (1973) and the equivalent considerations for diffuse planes and streaks are discussed by Boysen (1985). The case of 3D random disorder (incoherent neutron scattering, monotonous Laue scattering, averaged TDS, multiple scattering or short-range-order modulations) is treated by Sabine & Clarke (1977).

In polycrystalline samples the cross section has to be averaged over all orientations:

$$\frac{\mathrm{d}\sigma_\mathrm{p}}{\mathrm{d}\Omega}(\mathbf{H}') = \frac{n_\mathrm{c}}{H^2}\int \frac{\mathrm{d}\sigma}{\mathrm{d}\Omega}(\mathbf{H}') R'(|\mathbf{H}'| - |\mathbf{H}_0|)\,\mathrm{d}\mathbf{H}', \quad (4.2.8.11)$$

where n_c is number of crystallites in the sample; this averaged cross section enters the relevant expressions for the convolution product with the resolution function.

A general intensity expression may be written as (Boysen, 1985)

$$I_n(H_0) = P \sum_T m(T) A_n \Phi_n(H_0, T). \quad (4.2.8.12)$$

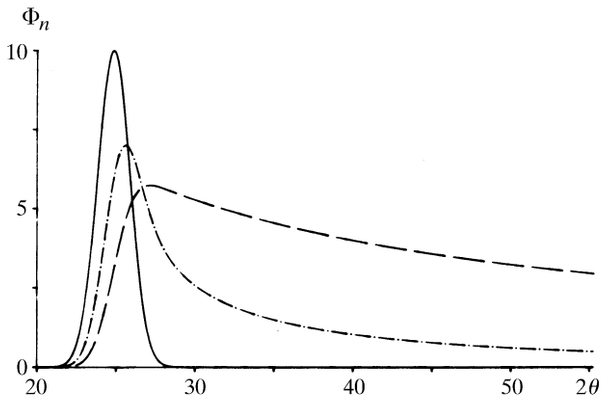

Fig. 4.2.8.2. Line profiles in powder diffraction for diffuse peaks (full line), continuous streaks (dot–dash lines) and continuous planes (broken lines). For explanation see text.

P denotes a scaling factor that depends on the instrumental luminosity, T is the shortest distance to the origin of the reciprocal lattice, $m(T)$ is the corresponding symmetry-induced multiplicity, A_n contains the structure factor of the structural units and the type of disorder, and Φ_n describes the characteristic modulation of the diffuse phenomenon of dimension n in the powder pattern. These expressions are given below with the assumption of Gaussian line shapes of width D for the narrow extension(s). The formulae depend on a factor $M = A_{1/2}(4k_1^2 - H_0^2)/(32\ln 2)$, where $A_{1/2}$ describes the dependence of the Bragg peaks on the instrumental parameters U, V and W (see Caglioti *et al.*, 1958),

$$A_{1/2}^2 = U\tan^2\theta + V\tan\theta + W, \qquad (4.2.8.13)$$

and $k_1 = 1/\lambda$.

(*a*) *Isotropic diffuse peak around T*

$$\Phi_0 = [2\pi(M^2 + D^2)]^{-1/2}(1/T^2) \times \exp\{-(H_0 - T)^2/2(M^2 + D^2)\}. \qquad (4.2.8.14)$$

The moduli $|\mathbf{H}_0|$ and T enter the exponential, *i.e.* the variation of $d\sigma/d\Omega$ along $|\mathbf{H}_0|$ is essential. For broad diffuse peaks ($M \ll D$) the angular dependence is due to $1/T^2$, *i.e.* proportional to $1/\sin^2\theta$. This result is valid for diffuse peaks of any shape.

(*b*) *Diffuse streak*

$$\Phi_1 = [2\pi(M^2 + D^2)]^{-1/2} \int_{-\infty}^{\infty} (T^2 + H^2)^{-1/2} \times \exp\{-H_0 - (T^2 + H^2)^{1/2}/2(M^2 + D^2)\}\,dH. \qquad (4.2.8.15)$$

The integral has to be evaluated numerically. If $(M^2 + D^2)$ is not too large, the term $1/(T^2 + H^2)$ varies only slowly compared to the exponential term and may be kept outside the integral, setting it approximately to $1/H_0^2$.

(*c*) *Diffuse plane (with $R^2 = H_x^2 + H_y^2$)*

$$\Phi_2 = (M^2 + D^2)^{-1/2} \int R^2/(T^2 + R^2) \times \exp\{-H_0 - (T^2 + R^2)^{1/2}/2(M^2 + D^2)\}\,dR. \qquad (4.2.8.16)$$

With the same approximation as in (*b*) the expression may be simplified to

$$\Phi_2 = \pi/H_0[1 - \mathrm{erf}\{(T - H_0)/[2(M^2 + D^2)]^{1/2}\} + 1/H_0^2[2\pi(M^2 + D^2)]^{1/2} \times \exp\{-(H_0 - T)^2/2(M^2 + D^2)\}]. \qquad (4.2.8.17)$$

(*d*) *Slowly varying diffuse scattering in three dimensions*

Φ_3 = constant. Consequently, the intensity is directly proportional to the cross section. The characteristic functions Φ_0, Φ_1 and Φ_2 are shown in Fig. 4.2.8.2 for equal values of T and D. Note the relative peak shifts and the high-angle tail.

4.2.8.3. Total diffraction pattern

As mentioned in Section 4.2.7.3.2, the atomic pair-distribution function (PDF), which is classically used for the analysis of the atomic distributions in liquids, melts or amorphous samples, can also be used to gain an understanding of disorder in crystals. The PDF is the Fourier transform of the total scattering. The measurement of total scattering is basically similar to recording X-ray or neutron powder patterns. The success of the method depends, however, decisively on various factors: (i) The availability of a large data set, *i.e.* reliable intensities up to high H values, in order to get rid of truncation ripples, which heavily influence the interpretation. Currently, values of $H_{\max}$ of more than 7 Å^{-1} can be achieved either with synchrotron X-rays [at the European Synchrotron Radiation Facility (ESRF) or Cornell High Energy Synchrotron Source (CHESS)] or with neutrons from reactors (*e.g.* instrument D4 at the ILL) and spallation sources [at ISIS or at LANSCE (instrument NPDF)]. (ii) High H resolution. (iii) High intensities, in particular at high H values. (iv) Low background of any kind which does not originate from the sample. High-quality intensities are therefore to be extracted from the raw data by taking care of an adequate absorption correction, correction of multiple-scattering effects, separation of inelastically scattered radiation (*e.g.* Compton scattering) and careful subtraction of 'diffuse' background which is not the 'true' diffuse scattering from the sample. These conditions are in practice rather demanding. A further detailed discussion is beyond the scope of this chapter, but a more thorough discussion is given, *e.g.*, by Egami (2004), and some examples are given by Egami & Billinge (2003).

References

Adlhart, W. (1981). *Diffraction by crystals with planar domains*. *Acta Cryst.* A**37**, 794–801.

Amorós, J. L. & Amorós, M. (1968). *Molecular Crystals: Their Transforms and Diffuse Scattering*. New York: John Wiley.

Arndt, U. W. (1986*a*). *X-ray position sensitive detectors*. *J. Appl. Cryst.* **19**, 145–163.

Arndt, U. W. (1986*b*). *The collection of single crystal diffraction data with area detectors*. *J. Phys. (Paris) Colloq.* **47**(C5), 1–6.

Aroyo, M. I., Boysen, H. & Perez-Mato, J. M. (2002). *Inelastic neutron scattering selection rules for phonons: application to leucite phase transitions*. *Appl. Phys. A*, **74**, S1043–S1048.

Axe, J. D. (1980). *Debye–Waller factors for incommensurate structures*. *Phys. Rev. B*, **21**, 4181–4190.

Bardhan, P. & Cohen, J. B. (1976). *X-ray diffraction study of short-range-order structure in a disordered Au_3Cu alloy*. *Acta Cryst.* A**32**, 597–614.

Bauer, G., Seitz, E. & Just, W. (1975). *Elastic diffuse scattering of neutrons as a tool for investigation of non-magnetic point defects*. *J. Appl. Cryst.* **8**, 162–175.

Bauer, G. S. (1979). *Diffuse elastic neutron scattering from nonmagnetic materials*. In *Treatise on Materials Science and Technology*, Vol. 15, edited by G. Kostorz, pp. 291–336. New York: Academic Press.

Berthold, T. & Jagodzinski, H. (1990). *Analysis of the distribution of impurities in crystals by anomalous X-ray scattering*. *Z. Kristallogr.* **193**, 85–100.

Bessière, M., Lefebvre, S. & Calvayrac, Y. (1983). *X-ray diffraction study of short-range order in a disordered Au_3Cu alloy*. *Acta Cryst.* B**39**, 145–153.

Beyeler, H. U., Pietronero, L. & Strässler, S. (1980). *Configurational model for a one-dimensional ionic conductor*. *Phys. Rev. B*, **22**, 2988–3000.